Nanoscale Res Lett (2009) 4:1130–1134
DOI 10.1007/s11671-009-9369-8

NANO EXPRESS

Nearly Monodispersion CoSm Alloy Nanoparticles Formed by an In-situ Rapid Cooling and Passivating Microfluidic Process

Yujun Song · Laurence L. Henry

Received: 25 March 2009 / Accepted: 28 May 2009 / Published online: 14 June 2009

Abstract An in situ *rapid cooling and passivating microfluidic process* has been developed for the synthesis of nearly monodispersed cobalt samarium nanoparticles (NPs) with tunable crystal structures and surface properties. This process involves promoting the nucleation and growth of NPs at an elevated temperature and rapidly quenching the NP colloids in a solution containing a passivating reagent at a reduced temperature. We have shown that Cobalt samarium NPs having amorphous crystal structures and a thin passivating layer can be synthesized with uniform nonspherical shapes and size of about 4.8 nm. The amorphous CoSm NPs in our study have blocking temperature near 40 K and average coercivity of 225 Oe at 10 K. The NPs also exhibit high anisotropic magnetic properties with a wasp-waist hysteresis loop and a bias shift of coercivity due to the shape anisotropy and the exchange coupling between the core and the thin oxidized surface layer.

Keywords Nanoparticles · Microfluidic reactor · Synthesis · Monodispersion · Alloy · Cobalt · Samarium

Over the years, microfluidic reactor (MR) processes have gained much attention in the preparation of specific materials due to its in situ spatial and temporal control of reaction kinetics, in addition to efficient mass and heat transfer [1–5]. Recently, application of microfluidic reactors has been expanded from the improvement of chemical reaction efficiency to the controlled synthesis of micro and nanoscale materials [4, 6–13]. Although significant progress has been achieved in size and shape control of NPs using microfluidic reactors, it is still challenging to obtain monodispersed NPs with controlled crystal structures [8]. One reason is possibly the difficulty in preventing aggregation and coarsening [caused by Ostwald Ripening (OR) and Oriented Attachment (OA) process and the concurrent phase transformation] of the NPs [8, 14]. These problems, aggregation and coarsening, often occurs in the bottled batch process and in MR processes if the growth of NPs is not carefully controlled. It is therefore important that process optimization be performed to suppress these processes, even in the MR process [8, 14–16]. According to the stability principle of NPs, elimination of defects in the crystal structure, passivation of the nanoparticle growth, and the deactivation of nanoparticle surfaces can be considered to suppress the OR and OA processes, and the in-time termination of nanoparticle aggregation [14].

A key goal in NP synthesis is control of the unique crystal structures and physical and chemical properties at different growth stages [10, 15]. However, it is difficult to achieve this by routine methods. In this article, an in situ rapid cooling and passivating microfluidic (IRCPM) process is presented in which the OR and OA process are suppressed, and the particle surfaces are deactivated. As shown in Fig. 1, the process includes three main areas: the mixing and reaction area, the nucleation and growth area, and the rapid cold quenching area. The mixing and reaction area includes one Y mixer (Y mixer 1). The delivery channels are designed as wedge shaped with inlet channels shrinking from 200 μm at the inputs to 30 μm at the ends,

Y. Song (✉)
Key Laboratory of Aerospace Materials and Performance (Ministry of Education), School of Materials Science and Engineering, Beihang University, 100191 Beijing, China
e-mail: yjsong2007@gmail.com; songyj@buaa.edu.cn

L. L. Henry
Department of Physics, Southern University A & M College, Baton Rouge, LA 70813, USA

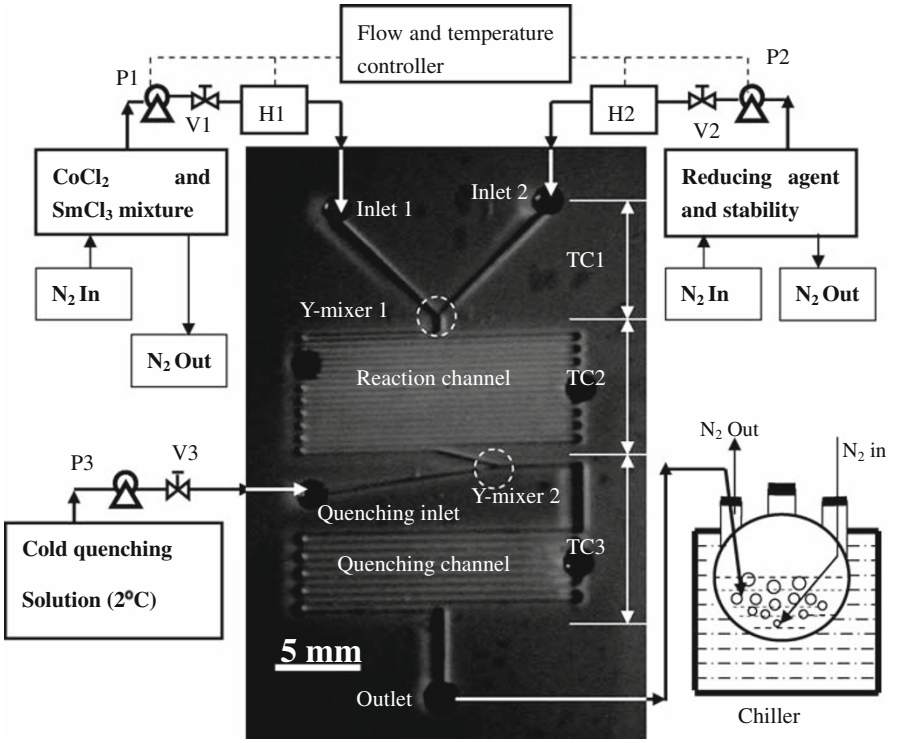

Fig. 1 The sequence temperature controlled microfluidic reactor process for Co_5Sm nanoparticle synthesis. The microfluidic reactor, fabricated by UV-LIGA process and sealed by semi-solid sealing process, is shown as the optical image in the center of the figure. The reactor consists of three regions: the mixing and reaction area from the inlets of 1 and 2 to Y mixers connected with channels shrinking from 200 to 30 μm, the nucleation and growth area with channel width of 60 μm and length of ~30 cm, and the rapid cold quenching area with the cold quenching solution delivered at the quenching solution inlet. The quenching solution mixes with the nanoparticle solution at Y mixer 2. The resulting mixture flows through the quenching channel (width of 120 μm and length of ~15 cm)

in order to realize a rapid mixing with low pressure loss. The nucleation and growth area has channel width of 60 μm and length of 30 cm. In the rapid cold quenching area, the cold quenching solution is delivered at the quenching solution inlet, to be mixed with the nanoparticle colloids at the Y mixer 2, following which the mix flows through the quenching channel. The quenching channel has a width of 120 μm and a length of 15 cm. The depth of all channels is ~600 μm, as determined from SEM image of the cross section of the micro channels (Fig. 2).

A typical reaction process is as follows: 25 mL of a mixture of $CoCl_2$ and $SmCl_3$ (28.5 mM $CoCl_2$, 5.7 mM $SmCl_3$ in tetrahydrofuran, THF) is delivered into a heater (H1) by a pump (P1), the mixture entering into the inlet 1 after it is heated to 50 °C. A volume of 25 mL of the reducing agent, which is a mixture of 90 mM $LiBEt_3H$ and 0.24 mM PVP in TH; PVP: Mw = 29,000, is delivered into a heater (H2) by a pump (P2), and heated to 52 °C before it is pumped into inlet 2. At the Y mixer 1, the salt mixture from inlet 1 mixes with the reducing agent, and the metal salts are rapidly reduced to metal atoms. The resulting metal atoms will nucleate and grow in the nucleation and growth area to form NPs at a constant temperature of 50 °C. When

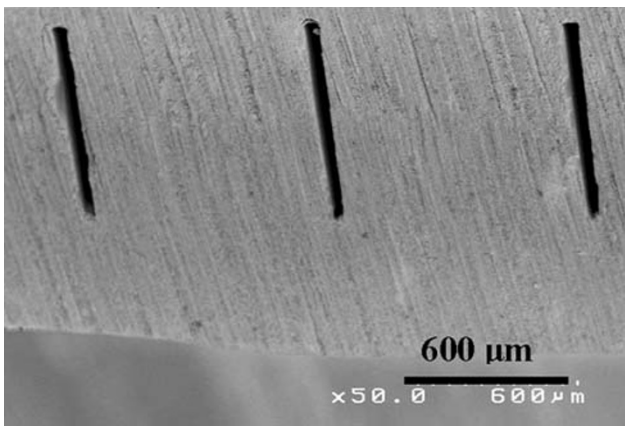

Fig. 2 The SEM image of the cross section of the channels. Based on the image, the channel width and depth were determined to be 60μm and 600 μm, respectively, suggesting a high depth/width ratio of ~10

the formed nanoparticle solution meets the cold quenching solution (2 °C, 10% acetone in THF) at the Y mixer 2, both the nanoparticle growth and the soon coming OR and OA processes can be suppressed, and the surfaces of NPs will be rapidly deactivated by acetone through a process of

suddenly forming an ultra-thin oxidation layer. When the nanoparticle solution is collected in the chiller-cooled receiver, both the nanoparticle growth and the OR and OA processes continue to be suppressed by the cold environment and the inert surfaces, until the particle synthesis is completed.

In order to see the advantage of the IRCPM process, the routine microfluidic process was also conducted by performing the quenching and collecting process at room temperature and without deactivating the nanoparticle surface. As expected, the formed NPs showed a broader dispersion with SD% greater than 15%. On the other hand, those NPs obtained by the IRCPM process have a SD% of about 8% (Fig. 3a, b). The NPs by IRCPM process show irregular but uniform shape (the inserted image in Fig. 3a), different from the spherical or ellipsoidal shapes obtained by the routine room temperature collecting process. It appears that the shape of the primary NPs would change to the spherical or ellipsoidal shape from their primary multifaceted shapes by OR and/or OA processes during the routine room temperature collecting process with a collecting time of greater than 5 h. The size of the NPs also increased slightly due to the two enhanced processes at room temperature. In the SAED pattern, the broad, diffuse rings, and the absence of diffraction spots indicate that the NPs obtained by IRCPM process have an amorphous structure (Fig. 3b). The amorphous phase for the 4.8 nm Co_5Sm NPs is likely due to the rapid cooling rate (calculated as 1.5×10^5 K/s based on a hot ball model), which will quickly freeze the crystal structure of NPs at 50 °C and slow down the OR and OA processes [17, 18]. The surface of the NPs can be rapidly deactivated through the formation of an ultra-thin oxidation layer caused by including acetone in the quenching solution. EDS data for the resulting NPs indicate the elemental oxygen appearing in those NPs (Fig. 3d). Analysis on the EDS spectrum of the CoSm alloy NPs also indicates that the alloy composition has reached the intended stoichiometry (Co/Sm = 5:1). The deactivated surfaces of the NPs together with the cold solution significantly slow the random growth of the NPs by OR and OA processes. A change in the coercivity (Hc) from −300 to 150 Oe in the hysteresis loop at 10 K (Fig. 4a) is also observed. This change is due to the exchange bias between the ferromagnetic Co_5Sm core and the antiferromagnetic oxidized surface [19]. A change in the coercivity is often observed in the ferromagnetic NPs with oxidized surfaces [19]. The zero-field-cooled (ZFC) and field-cooled (FC) magnetization measurements for the

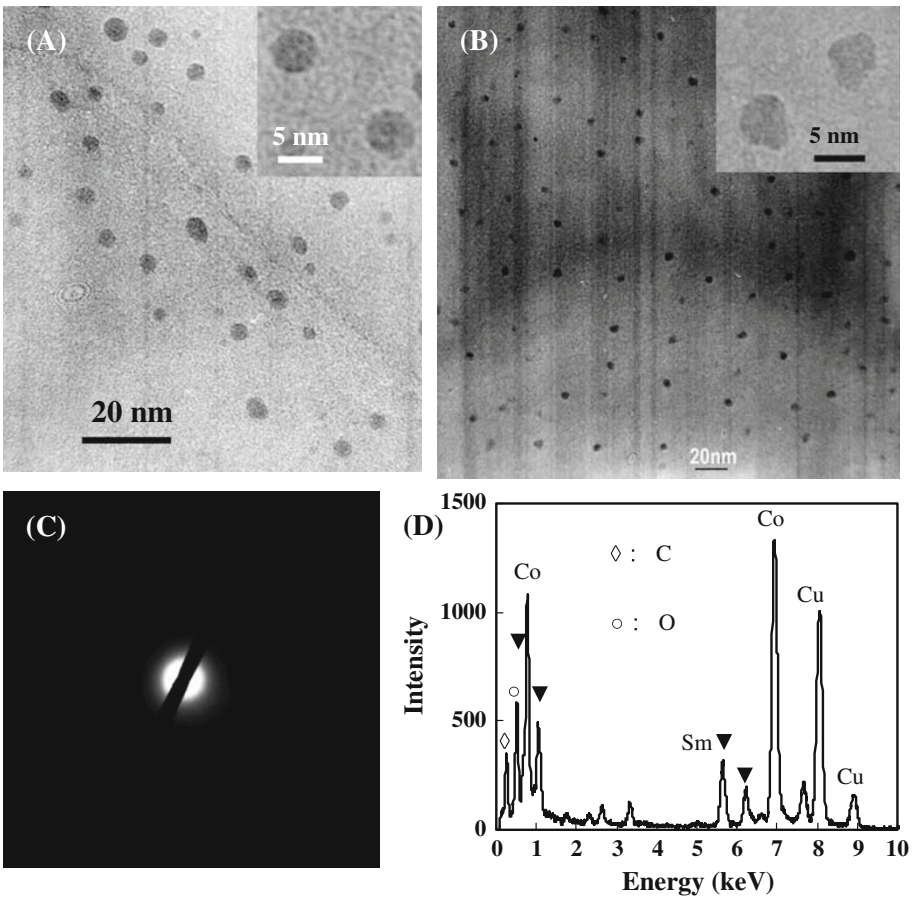

Fig. 3 The near monodispersion CoSm alloy nanoparticles synthesized by the microfluidic reactors. **a** The Co_5Sm nanoparticles collected under room temperature show ellipsoidal or spherical shape with broad size distribution of 5.1 ± 0.8 nm. **b** The as-synthesized Co_5Sm nanoparticles, cold quenched, mostly show nonspherical shape and uniform size of 4.8 ± 0.4 nm. **c** The SAED of CoSm alloy nanoparticles show dispersed rings, suggesting an amorphous phase. **d** The EDS spectrum of the CoSm alloy nanoparticles indicates alloy composition reaching the intended stoichiometry (Co/Sm = 5:1)

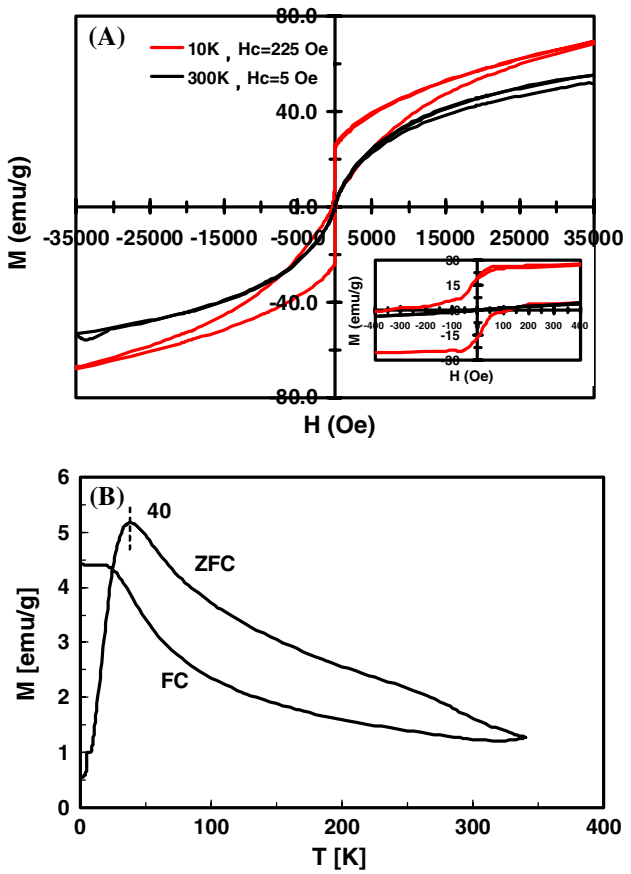

Fig. 4 The amorphous CoSm nanoparticles show a wasp-waist hysteresis loop at 10 K with an average coercivity of 225 Oe (right-bottom inserted image) and a Hc of 5 Oe at 300 K (**a**); the FC and ZFC magnetization curve of CoSm nanoparticles suggest a blocking temperature at 40 K (**b**)

NPs give a blocking temperature (Tb) of 40 K (Fig. 4b). The low Hc and Tb are most likely due to the unique amorphous crystal structures [20]. This is in contrast to the NPs synthesized by other methods, which show crystalline structure. In addition, our previous observations of Co NPs synthesized without further OR and OA processes also suggest a wasp-waist shaped hysteresis loop [21]. This is different from the crystal structure anisotropy occurring in spherical Co NPs [21]. The shape anisotropy due to the irregular morphologies of the Co_5Sm NPs (Fig. 3) may also contribute to this kind of hysteresis loop (Fig. 4).

In summary, nearly monodispersed amorphous Co_5Sm alloy NPs were fabricated by an IRCPM process. The resulting NPs retain their primary amorphous crystal structures and nonspherical shapes that are formed at elevated temperature without further Ostwald ripening and oriented attachment processes. The shape anisotropy and exchange coupling between the ferromagnetic core and the antiferromagnetic oxidized surface cause the NPs magnetic hysteresis loop at 10 K to show a wasp-waist character with a significant coercivity bias shift. To conclude, we have developed a method for producing nearly monodispersed magnetic CoSm NPs with desired structure and surface properties by using a rapid quenching technique.

Acknowledgments Author Y. Song is grateful for the financial support received from New Teacher Funds (2008-00061025) and SRF for ROCS and SEM by the Chinese Education Ministry, and Innovative Research Team of Chinese Education Ministry in University (IRT0512) at Beihang University. Y. Song also appreciates the kind suggestions from reviewers.

References

1. P. Watts, C. Wiles, Recent advances in synthetic micro reaction technology. Chem. Commun. (Camb) **5**, 443–467 (2007). doi:10.1039/b609428g
2. T.L. Sounart, P.A. Safier, J.A. Voigt, J. Hoyt, D.R. Tallant, C.M. Matzke, T.A. Michalske, Spatially-resolved analysis of nanoparticle nucleation and growth in a microfluidic reactor. Lab Chip **7**, 908–915 (2007)
3. H. Pennemann, P. Watts, S.J. Haswell, V. Hessel, H. Lowe, Benchmarking of microreactor applications. Org. Process. Res. Dev. **8**, 422–439 (2004). doi:10.1021/op0341770
4. A.J. deMello, Control and detection of chemical reactions in microfluidic systems. Nature **442**, 394–402 (2006). doi:10.1038/nature05062
5. H.R. Sahoo, J.G. Kralj, K.F. Jensen, Multistep continuous-flow microchemical synthesis involving multiple reactions and separations. Angew. Chem. Int. Ed. **46**, 5704–5708 (2007). doi:10.1002/anie.200701434
6. J. Boleininger, A. Kurz, V. Reuss, C. Sonnichsen, Microfluidic continuous flow synthesis of rod-shaped gold and silver nanocrystals. Phys. Chem. Chem. Phys. **8**, 3824–3827 (2006). doi:10.1039/b604666e
7. Y. Song et al., Shape and crystallinity shift of nanoparticles formed in a microfluidic reactor. J. Nanopart. Res. (under reviewing)
8. Y. Song, T. Zhang, W.T. Yang, S. Albin, L.L. Henry, Fine crystal structure transition of cobalt nanoparticles formed in a microfluidic reactor. Cryst. Growth. Des. **8**, 3766–3772 (2008). doi:10.1021/cg8003992
9. J.B. Edel, R. Fortt, J.C. deMello, A.J. deMello, Microfluidic routes to the controlled production of nanoparticles. Chem. Comm. **10**, 1136–1137 (2002)
10. S. Krishnadasan, R.J.C. Brown, A.J. deMello, J.C. deMello, Intelligent routes to the controlled synthesis of nanoparticles. Lab Chip **7**, 1434–1441 (2007). doi:10.1039/b711412e
11. L.-H. Hung, A.P. Lee, Microfluidic devices for the synthesis of nanoparticles and biomaterials. J. Med. Biol. Eng. **27**, 1–6 (2007)
12. A. Jahn et al., Preparation of nanoparticles by continuous-flow microfluidics. J. Nanopart. Res. **10**, 925–934 (2008). doi:10.1007/s11051-007-9340-5
13. Y. Song, C.S.S.R. Kumar, J. Hormes, Synthesis of palladium nanoparticles using a continuous flow polymeric micro reactor. J. Nanosci. Nanotechnol. **4**, 788–793 (2004). doi:10.1166/jnn.2004.111
14. B. Gilbert et al., Special phase transformation and crystal growth pathways observed in nanoparticles. Geochem. Trans. **4**, 20–27 (2003). doi:10.1186/1467-4866-4-20
15. Y. Song, C.S.S.R. Kumar, J. Hormes, Microfluidic synthesis of nanomaterials. Small **4**, 698–711 (2008). doi:10.1002/smll.200701029

16. C. Ribeiro, E.J.H. Lee, E. Longo, E.R. Leite, A kinetic model to describe nanocrystal growth by the oriented attachment mechanism. Chem. Phys. Chem. **6**, 690–696 (2005). doi:10.1002/cphc.200400505
17. H.S. Carslaw, J.C. Jaeger, *Conduction of heat in solids* (Clarendon Press, Oxford, 1956), p. 232
18. J.H.I. Lienhard, *Lienhard JHV A heat transfer textbook* (Phkigiston Press, Massachusetts, 2003), pp. 203–223
19. S.E. Inderhees et al., Manipulating the magnetic structure of Co core/CoO shell nanoparticles: implications for controlling the exchange bias. Phys. Rev. Lett. **101**, 117202 (2008). doi:10.1103/PhysRevLett.101.117202
20. E.M. Kirkpatrick, S.A. Majetich, M.E. McHenry, Magnetic properties of single domain samarium cobalt nanoparticles. IEEE Trans. Magn. **32**, 4502–4504 (1996). doi:10.1109/20.538911
21. Y. Song, L.L. Henry, W.T. Yang, In situ rapid cooling microfluidic process for the formation of stable cobalt amorphous nanoparticles Langmuir (revised reversion under reviewing)